

QCD analysis of diffractive phenomena ^{*}

LAURENT SCHOEFFEL

CEA Saclay/DAPNIA-SPP, 91191 Gif-sur-Yvette, France

The most important results on subnuclear diffractive phenomena obtained at HERA and Tevatron are reviewed and new issues in nucleon tomography are discussed. Some challenges for understanding diffraction at the LHC, including the discovering of the Higgs boson, are outlined.

1. Introduction

One of the most important experimental results from the DESY electron-proton collider HERA, working at a center of mass energy of about 300 GeV, is the observation of a significant fraction, around 15%, of large rapidity gap events in deep inelastic scattering (DIS). In these events, the target proton emerges in the final state with a loss of a very small fraction ($x_{\mathbb{P}}$) of its energy-momentum [1].

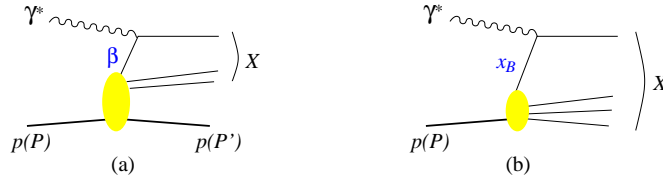


Fig. 1. Parton model diagrams for deep inelastic diffractive (a) and inclusive (b) scattering observed at lepton-proton collider HERA. The variable β is the momentum fraction of the struck quark with respect to $P - P'$, and the Bjorken variable x_{Bj} its momentum fraction with respect to P .

In Fig. 1(a), we present this event topology, $\gamma^* p \rightarrow X p'$, where the virtual photon γ^* probes the proton structure and originates from the electron. Then, the final hadronic state X and the scattered proton are well separated in space (or rapidity) and a gap in rapidity can be observed in the event with no particle produced between X and the scattered proton. In

^{*} Presented at PIC, Annecy, France, 26 - 29 june 2007

the standard QCD description of DIS, such events are not expected in such an abundance since large gaps are exponentially suppressed due to color strings formed between the proton remnant and scattered partons (see Fig. 1(b)). The theoretical description of these processes, also called diffractive processes, is a real challenge since it must combine perturbative QCD effect of hard scattering with nonperturbative phenomenon of rapidity gap formation [2]. The name diffraction in high-energy particle physics originates from the analogy between optics and nuclear high-energy scattering. In the Born approximation the equation for hadron-hadron elastic scattering amplitude can be derived from the scattering of a plane wave passing through and around an absorbing disk, resulting in an optic-like diffraction pattern for hadron scattering. The quantum numbers of the initial beam particles are conserved during the reaction and then the diffractive system is well separated in rapidity from the scattered hadron.

The discovery of large rapidity gap events at HERA has led to a renaissance of the physics of diffractive scattering in an entirely new domain, in which the large momentum transfer provides a hard scale. This observation has also revived the the rapidity gap physics with hard triggers, as large- p_{\perp} jets, at the proton-antiproton collider Tevatron, currently working at a center of mass energy of about 2 TeV (see Fig. 2) [1, 2].

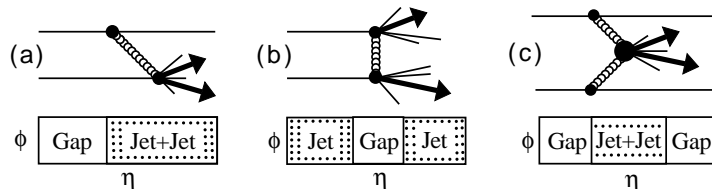


Fig. 2. Schematic diagrams of topologies representative of hard diffractive processes studied by the proton-antiproton collider Tevatron.

Whether the existence of such hard scales makes the diffractive processes tractable within the perturbative QCD or not has been a subject of intense theoretical and experimental research during the past decade. In the following, we describe the main ideas and results. Using the standard vocabulary, the vacuum/colorless exchange involved in the diffractive interaction is called Pomeron in this paper.

2. Basics of diffractive interactions

The inclusive diffractive cross section has been measured at HERA by H1 and ZEUS experiments over a wide kinematic range, as illustrated in Fig. 3. We observe that the diffractive cross section shows a hard dependence in the centre-of-mass energy of the γ^*p system W . Namely, we get a behaviour

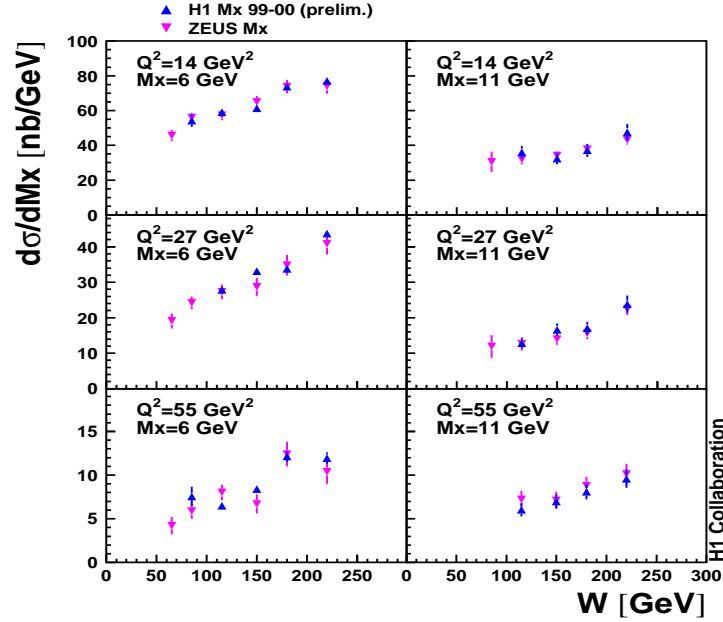


Fig. 3. The cross section of the diffractive process $\gamma^* p \rightarrow p' X$, differential in the mass of the diffractively produced hadronic system X (M_X), is presented as a function of the centre-of-mass energy of the $\gamma^* p$ system W . Measurements at different values of the virtuality Q^2 of the exchanged photon are displayed.

of the form $\sim W^{0.6}$ for the diffractive cross section, compatible with the dependence expected for a hard process. This first observation allows further studies of the diffractive process in the context of perturbative QCD.

Several theoretical formulations have been proposed to describe the diffractive exchange. The purpose here is to describe the "blob" displayed in Fig. 1(a) in a quantitative way, leading to a proper description of data shown in Fig. 3. Among the most popular models, the one based on a point-like structure of the Pomeron assumes that the exchanged object, the Pomeron, is a colour-singlet quasi-particle whose structure is probed in the reaction. In this approach, diffractive parton distribution functions (PDFs) are derived from the diffractive DIS cross sections in the same way as standard PDFs are extracted from DIS measurements [2]. It means that a certain flux of Pomeron is emitted off the proton, depending on the variable x_P , the fraction of the

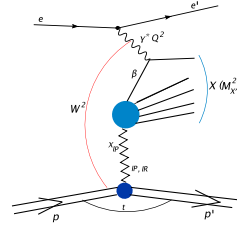


Fig. 4. Kinematics.

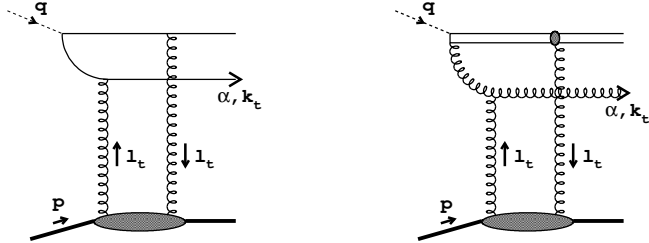


Fig. 5. The $q\bar{q}$ and $q\bar{q}g$ components of the diffractive system.

longitudinal momentum of the proton lost during the interaction (see Fig. 4). Then, the partonic structure of the Pomeron is probed by the diffractive exchange (see Fig. 1(a) and 4). In Fig. 4, we illustrate this factorisation property and remind the notations for the kinematic variables used in this paper, as the virtuality Q^2 of the exchanged photon, the centre-of-mass energy of the γ^*p system W and M_X the mass of the diffractively produced hadronic system X . It follows that the Bjorken variable x_{Bj} verifies $x_{Bj} \simeq Q^2/W^2$ in the low x_{Bj} of the H1/ZEUS measurements ($x_{Bj} < 0.01$). Also, the Lorentz invariant variable β defined in Fig. 1 is equal to $x_{Bj}/x_{\mathbb{P}}$ and can be interpreted as the fraction of longitudinal momentum of the struck parton in the (resolved) Pomeron.

This resolved Pomeron model gives a good description of HERA data but fails to describe the Tevatron results. Indeed, some underlying interactions can occur during the proton-antiproton collision, which break the gap in rapidity produced in the diffractive process [1].

3. Dipole model of diffractive interactions

In the following, we focus our discussion on a different approach of diffractive interactions in which the process is modeled with the exchange of (at least) two gluons projected onto the color singlet state (see Fig. 5) [3, 4]. In this model, the reaction follows three different phases displayed in Fig. 5 : (i) the transition of the virtual photon to the $q\bar{q}$ pair (the color dipole) at a large distance $l \sim \frac{1}{m_N x}$ of about 10-100 fm for HERA kinematics, upstream the target, (ii) the interaction of the color dipole with the target nucleon, and (iii) the projection of the scattered $q\bar{q}$ onto the diffractive system X .

The inclusive diffractive cross section is then described with three main contributions [5]. The first one describes the diffractive production of a $q\bar{q}$ pair from a transversely polarised photon, the second one the production of a diffractive $q\bar{q}g$ system, and the third one the production of a $q\bar{q}$ component from a longitudinally polarised photon (see Fig. 5). In Fig. 6, we show that

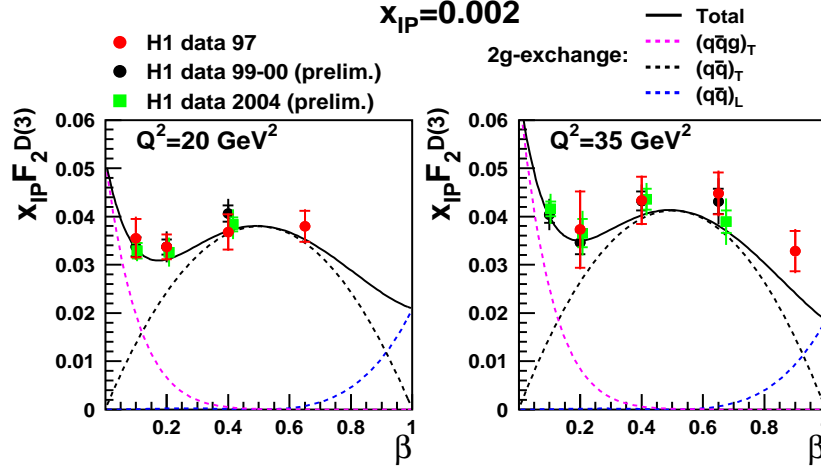


Fig. 6. The diffractive structure function $x_{\mathbb{P}} F_2^{D(3)}$ is presented as a function of β for two values of Q^2 . The different components of the two-gluon exchange model are displayed (see text). They add up to give a good description of the data. The structure function $x_{\mathbb{P}} F_2^{D(3)}$ is obtained directly from the measured diffractive cross section using the relation : $\frac{d^3 \sigma^{ep \rightarrow eXp}}{dx_{\mathbb{P}} dx dQ^2} \simeq \frac{4\pi\alpha_{em}^2}{xQ^4} (1 - y + \frac{y^2}{2}) F_2^{D(3)}(x_{\mathbb{P}}, x, Q^2)$, where y represents the inelasticity of the reaction.

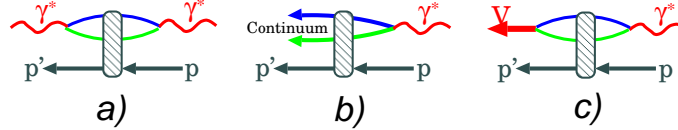


Fig. 7. The unified picture of Compton scattering, diffraction excitation of the photon into hadronic continuum states and into the diffractive vector meson

this two-gluon exchange model gives a good description of the diffractive cross section measurements.

One of the great interest of the two-gluon exchange approach is that it provides a unified description of different kind of processes measured in $\gamma^* p$ collisions at HERA [6] : inclusive $\gamma^* p \rightarrow X$, diffractive $\gamma^* p \rightarrow X p'$ and (diffractive) exclusive vector mesons (VM) production $\gamma^* p \rightarrow VM p'$ (see Fig. 7). In the last case, the step (iii) described above consists in the recombination of the scattered pair $q\bar{q}$ onto a real VM (as J/Ψ , ρ^0 , ϕ , ...) or onto a real photon for the reaction $\gamma^* p \rightarrow \gamma p'$, which is called deeply virtual Compton scattering (DVCS).

The dipole model then predicts a strong rise of the cross section in W , which reflects the rise at small x_{Bj} of the gluon density in the proton. Indeed, in the two-gluon exchange model, the exclusive VM production cross section can be simply expressed as proportional to the square of the gluon density. At low x_{Bj} , the gluon density increases rapidly when x_{Bj} decreases and therefore a rapid increase of the cross section with W is expected and observed (see Fig. 8). Note that saturation effects, that are screening the large increase of the dipole cross section (gluon density) at low x_{Bj} , are taken into account in recent developments of the dipole approach. Also, skewing effects are included in models, i.e. the difference between the proton momentum fractions carried by the two exchanged gluons. The gluon density is then replaced by a generalized parton distribution, labeled F_g in the following. The VM cross section is then related to the square of F_g . Finally, a reasonable agreement with the data is obtained (see Fig. 8) [6, 7].

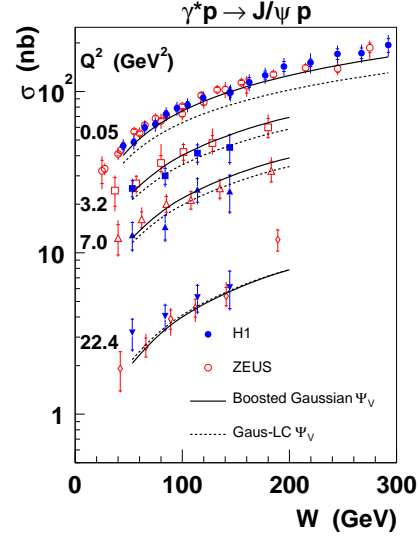


Fig. 8. J/Ψ exclusive production cross section as a function of W for different Q^2 values compared to predictions from a dipole model (including saturation and skewing effects). Two different vector meson wave functions are used corresponding to the two curves.

4. Nucleon tomography

One of the key measurement in exclusive processes is the slope defined by the exponential fit to the differential cross section: $d\sigma/dt \propto \exp(-b|t|)$ at small t , where $t = (p - p')^2$ is the square of the momentum transfer at the proton vertex (see Fig. 9). A Fourier transform from momentum to impact parameter space readily shows that the t -slope b is related to the typical transverse distance between the colliding objects [8, 9]. At high scale, the $q\bar{q}$ dipole is almost point-like, and the t dependence of the cross section is given by the transverse extension of the gluons (or sea quarks) in the proton for a given x_{Bj} range. More precisely, from the generalised gluon distribution F_g defined in section 3, we can compute a gluon density

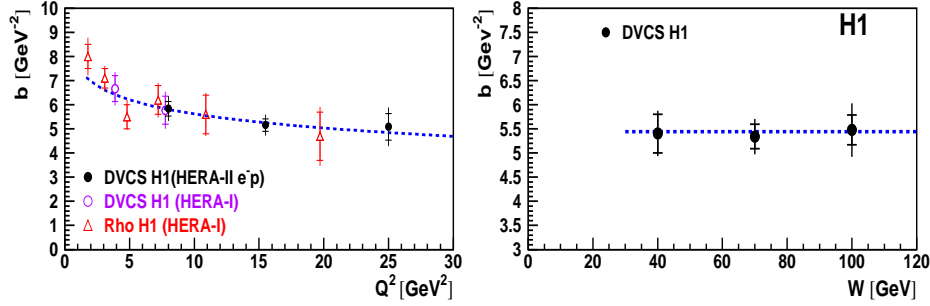


Fig. 9. The logarithmic slope of the t dependence for DVCS and ρ exclusive production : $d\sigma/dt \propto \exp(-b|t|)$ where $t = (p - p')^2$.

which also depends on a spatial degree of freedom, the transverse size (or impact parameter), labeled R_\perp , in the proton. Both functions are related by a Fourier transform

$$g(x, R_\perp; Q^2) \equiv \int \frac{d^2 \Delta_\perp}{(2\pi)^2} e^{i(\Delta_\perp R_\perp)} F_g(x, t = -\Delta_\perp^2; Q^2).$$

Thus, the transverse extension $\langle r_T^2 \rangle$ of gluons (or sea quarks) in the proton can be written as

$$\langle r_T^2 \rangle \equiv \frac{\int d^2 R_\perp g(x, R_\perp) R_\perp^2}{\int d^2 R_\perp g(x, R_\perp)} = 4 \frac{\partial}{\partial t} \left[\frac{F_g(x, t)}{F_g(x, 0)} \right]_{t=0} = 2b$$

where b is the exponential t -slope. Measurements of b have been performed for different channels, as DVCS or ρ production (see Fig. 9-left-), which corresponds to $\sqrt{r_T^2} = 0.65 \pm 0.02$ fm at large scale Q^2 for $x_{Bj} \simeq 10^{-3}$ [10, 11]. This value is smaller than the size of a single proton, and, in contrast to hadron-hadron scattering, it does not expand as energy W increases (see Fig. 9-right-). This result is consistent with perturbative QCD calculations in terms of a radiation cloud of gluons and quarks emitted around the incoming virtual photon.

5. Quarks total angular momenta

In section 3, we have introduced the generalised parton distributions (GPDs) in the presence of skewing, difference of momenta between the two exchanged gluons or quarks. These functions have interesting features : they interpolate between the standard PDFs and hadronic form factors. Also, they complete the nucleon spin puzzle as they provide a measurement of the total angular momentum contribution of any parton to the nucleon

spin [12]. In the DVCS process, the skewing is large. It can be shown that the difference of momenta between the two exchanged partons reads : $\delta(x) = x_{Bj}/(2 - x_{Bj})$. That's why it is a golden reaction to access GPDs, in particular when measuring its interference with the non-discernable (electromagnetic) Bethe-Heitler (BH) process.

Following this strategy, different asymmetries can be extracted [10, 11, 13], which depend on the helicity/charge of the beam particles or on the polarisation of the target. These asymmetries are then directly related to the DVCS/BH interference, hence directly sensitive to GPDs. The HERMES collaboration, which is a fixed target experiment using the 27.6 GeV electron beam of HERA, has completed recently a measurement directly sensitive to the u and d quarks angular momenta [14]. The result is given in Fig. 10 where for the first time a constraint in the plane J_u/J_d can be derived [14].

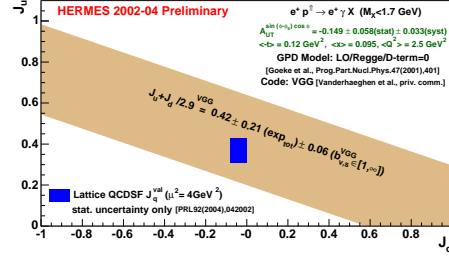


Fig.10. Constraint on u -quark total angular momentum J_u vs d -quark total angular momentum J_d , obtained at HERMES. Also shown is a Lattice result.

6. Towards LHC

In recent years, the production of the Higgs boson in diffractive proton-proton collisions at the LHC has drawn more and more attention as a clean channel to study the properties of a light Higgs boson or even discover it. This is an interesting example of a new challenge. The idea is to search for exclusive events at the LHC, as illustrated in Fig. 2(c) [15, 16]. The full energy available in the center of mass is then used to produce the heavy object, which can be a dijet system, a W boson or could be a Higgs boson. With this topology, the event produced is very clean : both protons escape and are detected in forward Roman pot detectors, two large rapidity gaps are created on both sides and the central production of the heavy object gives some decay products well isolated in the detector (see Fig. 2(c)). A second advantage of such events is that the resolution on the mass of the produced object can be determined with a high resolution from the measurement of the proton momentum losses ($x_{\mathbb{P},1}$ and $x_{\mathbb{P},2}$), using the relation $M^2 = s x_{\mathbb{P},1} x_{\mathbb{P},2}$ where \sqrt{s} is the center of mass energy available in the collision. A potential signal, accessible in a mass distribution, is then not washed out by the lower resolution when using central detectors, rather than forward Roman pots to measure $x_{\mathbb{P},1}$ and $x_{\mathbb{P},2}$ [15, 16].

7. Conclusions

We have presented and discussed the most recent results on diffraction from the HERA and Tevatron experiments. With exclusive processes studies, we have shown that a scattering system consisting of a small size vector particle and the proton has a transverse extension (at high scale) smaller than a single proton and does not expand as energy increases. This result is consistent with perturbative QCD calculations in terms of a radiation cloud of gluons and quarks emitted around the incoming virtual photon. Of special interest for future prospects is the exclusive production heavy objects (including Higgs boson) at the LHC.

REFERENCES

- [1] C. Royon, Acta Phys. Polon. B **37** (2006) 3571 [hep-ph/0612153].
- [2] C. Royon, L. Schoeffel, S. Sapeta, R. Peschanski and E. Sauvan, hep-ph/0609291 ; Nucl. Phys. B **746** (2006) 15 [hep-ph/0602228].
- [3] A.H. Mueller, Nucl. Phys. **B335** (1990) 115; N.N. Nikolaev and B.G. Zakharov, Zeit. für. Phys. **C49** (1991) 607.
- [4] A. Bialas and R. Peschanski, Phys. Lett. **B378** (1996) 302 [hep-ph/9512427]; Phys. Lett. **B387** (1996) 405 [hep-ph/9605298]; S. Munier, R. Peschanski and C. Royon, Nucl. Phys. **B534** (1998) 297 [hep-ph/9807488].
- [5] J. Bartels, J. R. Ellis, H. Kowalski and M. Wusthoff, Eur. Phys. J. C **7** (1999) 443 [hep-ph/9803497].
- [6] I. P. Ivanov, N. N. Nikolaev and A. A. Savin, Phys. Part. Nucl. **37** (2006) 1 [hep-ph/0501034].
- [7] H. Kowalski and D. Teaney, Phys. Rev. D **68** (2003) 114005 [hep-ph/0304189]; J. Bartels and H. Kowalski, Eur. Phys. J. C **19** (2001) 693 [hep-ph/0010345].
- [8] M. Burkardt, Int. J. Mod. Phys. A **18** (2003) 173 [hep-ph/0207047].
- [9] M. Diehl, Eur. Phys. J. C **25** (2002) 223 [Erratum-ibid. C **31** (2003) 277] [hep-ph/0205208].
- [10] L. Schoeffel, proceedings DIS 2007, 0705.2925 [hep-ph].
- [11] L. Schoeffel, arXiv:0706.3488 [hep-ph].
- [12] X. D. Ji, Phys. Rev. D **55** (1997) 7114 [hep-ph/9609381].
- [13] A. Airapetian *et al.* [HERMES Collaboration], Phys. Rev. D **75** (2007) 011103 [hep-ex/0605108].
- [14] F. Ellinghaus, W. D. Nowak, A. V. Vinnikov and Z. Ye, Eur. Phys. J. C **46** (2006) 729 [hep-ph/0506264]; Z. Ye [HERMES Collaboration], Proceedings DIS 2006, hep-ex/0606061.
- [15] C. Royon [RP220 Collaboration], 0706.1796 [physics.ins-det].
- [16] L. Schoeffel, proceedings PHOTON 2007, 0707.3199 [hep-ph]; proceedings Moriond QCD 2007, 0705.1413 [hep-ph].